Progress In Electromagnetics Research, Vol. 114, 17–32, 2011

EXTENDED WAVENUMBER DOMAIN ALGORITHM FOR HIGHLY SQUINTED SLIDING SPOTLIGHT SAR DATA PROCESSING

D. M. Guo, H. P. Xu, and J. W. Li

School of Electronic and Information Engineering
Beihang University, Beijing, China

Abstract—Image formation from squinted sliding spotlight synthetic aperture radar (SAR) is limited by azimuth spectral folding and severe two dimension coupling. This paper presents an Extended Wavenumber Domain Algorithm (WDA) for highly squinted sliding spotlight SAR data processing. This algorithm adopts azimuth deramping approach to overcome the azimuth spectral folding phenomenon. The chirp rate for azimuth deramping and the principle of choosing pulse repetition frequency (PRF) is presented to accommodate the characteristic of Doppler history. Subsequently, the full focusing is implemented by WDA. Instead of the conventional Stolt mapping in WDA, a modified Stolt mapping is introduced in order to enlarge the range extension of focused image and enable to update the Doppler parameters along range. To confirm the correctness of the implementation of modified Stolt mapping and the azimuth position of target in focused image, related compensation terms are developed. Point target simulation results are presented to validate the effectiveness of extended WDA to process highly squinted sliding spotlight SAR data.

1. INTRODUCTION

Synthetic aperture radar (SAR) is an invaluable tool for remote sensing applications [1–5]. In order to satisfy the demand that SAR systems possess the capability to image with high resolution and wide swath, an innovative sliding spotlight mode, originally called hybrid stripmap/spotlight mode, was proposed in [6]. In this operation mode, the radar antenna beam is steered about a point further away from the

Received 20 January 2011, Accepted 14 February 2011, Scheduled 16 February 2011
Corresponding author: De Ming Guo (demingguo@ee.buaa.edu.cn).

radar than the area being illuminated. Consequently, the contradiction between the azimuth resolution and coverage extension, which restricts the performance of the well-known strip-map and spotlight mode, is efficiently solved. But the elaborate steering of the antenna (either mechanically or electronically) results in an adverse phenomenon that the total azimuth signal bandwidth might span over several pulse repetition frequency (PRF) intervals (i.e., azimuth spectral folding phenomenon). This limits the straightforward application of available strip-map imaging algorithm [7–10] to process sliding spotlight SAR data. Although the polar format algorithm [11] based on dechirp receive technique eliminates the azimuth spectral folding, it is only suitable for spotlight SAR imaging. Three rational approaches have been proposed to overcome the azimuth spectral folding and extend the focusing capability of conventional strip-map imaging algorithm. They are sub-apertures [12, 13], azimuth up-sampling [14] and azimuth deramping [15, 16] respectively. The necessary overlap between sub-apertures and complicated recombination degrade the processing efficiency of sub-apertures approach. In terms of up-sampling approach, vast zero padding increases computation load. Compared with the aforementioned two approach, azimuth deramping is more efficient due to the fast implementation of its space-invariant azimuth filtering.

The existing analysis and imaging algorithms of sliding spotlight SAR are all for broadside mode, where the pointing direction of the antenna beam is perpendicular to the flight path at the azimuth center time. Oppositely, the SAR system is working with squint mode, when there is an offset angle between the pointing direction of the antenna and the zero Doppler plane at azimuth center time. Compared with broadside mode, the squint mode can increase the flexibility of SAR system, provide information about surface structure through the measurement of the azimuth angle dependence of backscatter and enlarge the extension of azimuth focused scene within a single imaging. Thus the investigation on squint sliding spotlight SAR is especially significant. However, current squint mode imaging algorithms is merely for strip-map mode, such as extended chirp scaling (ECS) algorithms [17], nonlinear CS (NCS) algorithms [18], azimuth nonlinear chirp scaling (NLCS) algorithm based on range walk removal [19], wavenumber domain algorithm (WDA) [21], and the algorithms based on sub-aperture formation [20]. The ECS algorithm is only suitable for processing data under middle squint angle because of ignoring the range-dependent property of second range compression (SRC) term. The NLCS algorithm loses the azimuth invariant property owing to the range walk removal, and thus the size of focused scene

and image resolution must be restricted. The processing efficiency of the algorithms based on sub-aperture formation is still degraded due to its overlap and recombination. NCS and WDA are effective algorithms to focus high resolution and highly squinted SAR data. The NCS algorithm eliminates the range-variant property of SRC, but it ignores the cubic phase term's effect to the stationary point during its derivation and the process flow is comparatively complex. The WDA is the best precise frequency-domain imaging algorithm, but it needs the interpolation to implement Stolt mapping, which mainly determines the precision and efficiency of WDA.

This paper presents an extended WDA for highly squinted sliding spotlight SAR data processing. This algorithm combines the advantages of the efficient azimuth deramping and precise WDA. Although the azimuth deramping is inherited from Lanari [15], the peculiarity of squint sliding spotlight SAR data is taken into account in particular. By exactly analyzing the characteristics of the squint sliding spotlight SAR echo signal, the expression of the rate of the Doppler centroid varying is precisely derived. Based on this expression, azimuth deramping is introduced to overcome the azimuth spectral folding. Furthermore, considering the characteristic of Doppler history and azimuth extension in focused image, the principle of choosing system PRF is particularly discussed. Improved WDA is applied to implement the residual and precise focusing of highly squinted sliding spotlight SAR data. In order to enlarge the range extension in focused image and enable the motion compensation, modified Stolt mapping of WDA in [21] is introduced and further improved. Considering that the Stolt mapping is efficiently implemented by sinc interpolation, which requires that the signal is bandlimited, the phase term for match filtering is modified. Moreover, a time-shift term is incorporated into the azimuth compression in order to correct the azimuth position aberration of target, which is arising from the Doppler centroid and azimuth deramping.

This paper is organized as follows. Section 2 analyzes the signal characteristic of squint sliding spotlight SAR echo data. Section 3 presents the implementation of extended WDA. Section 4 presents the point target simulation results to validate the effectiveness of the proposed algorithm. Finally, Conclusions are summarized in Section 5.

2. SIGNAL CHARACTERISTIC OF ECHO DATA

The 3-dimension acquisition geometry of squint sliding spotlight SAR is shown in Figure 1. We define the inertial coordinate system $OXYZ$, the origin is the nadir at azimuth center time, the x-axis points along

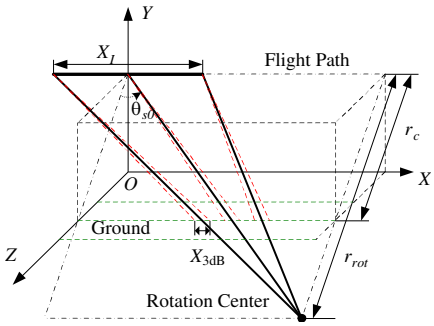

Figure 1. Acquisition geometry of squint sliding spotlight mode.

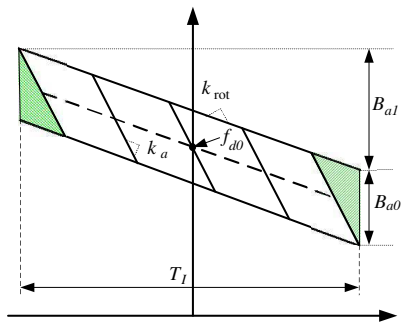

Figure 2. Time-frequency diagram of squint sliding spotlight mode.

flight path, the y-axis is perpendicular to the ground plane, and the z-axis accomplishes a right-hand Cartesian coordinate system. During the flight, the antenna beam is always steered about the ideal rotation center located under the ground level. The total observation length is X_I, and the corresponding observation time is $T_I = X_I/v$. The azimuth antenna beam footprint is $X_{3\text{dB}}$. The squint angle at azimuth center time, defined as the angle between the radar light of sight (LOS) and the zero Doppler plane, is θ_{s0}. The closest range between flight path and scene center is r_c, and the closest range between flight path and the rotation center is r_{rot}. At azimuth center time, the slant range between antenna phase center (APC) and scene center is $R_{c0} = r_c/\cos\theta_{s0}$, and the slant range between APC and rotation center is $R_{rot0} = r_{rot}/\cos\theta_{s0}$.

The mode factor can be defined as

$$A = \frac{r_{rot} - r_c}{r_{rot}} = \frac{R_{rot0} - R_{c0}}{R_{rot0}} \tag{1}$$

Generally, this factor should satisfy $X/X_I \leq A \leq 1$. And note that, this definition ignores the slightly range-dependent property of mode factor. Compared with strip-map mode, the azimuth resolution of sliding spotlight mode is A times.

The echo signal of a point target located at $(r, t_0 + t_n)$ can be expressed as

$$\begin{aligned} & ss\left(\tau, t; r, t_n\right) \\ = \ & \text{rect}\left[\frac{\tau - 2R(t;r,t_n)/c}{T_p}\right] \exp\left\{-j\pi K_r\left[\tau - \frac{2R(t;r,t_n)}{c}\right]^2\right\} \\ & \cdot\text{rect}\left[\frac{t}{T_I}\right] \text{rect}\left[\frac{Avt - vt_n}{X_{3\text{dB}}}\right] \exp\left\{-j\frac{4\pi R(t;r,t_n)}{\lambda}\right\} \end{aligned} \tag{2}$$

where r is the closest range between flight path and point target, t_0 is the zero Doppler time of scene center, $t_0 = r_c \tan\theta_{s0}/v$, t_n is the difference of zero Doppler time between scene center and point target, τ is the range fast time, t is the azimuth slow time, T_p is the transmitted pulse width, c is the speed of electromagnetic wave, K_r is the chirp rate of transmitted signal, v is the velocity of sensor, λ is the wavelength, and $R(t; r, t_n)$ is the slant range history during the entire observation time, which is given by

$$R(t; r, t_n) = \sqrt{r^2 + v^2 (t - t_0 - t_n)^2} \tag{3}$$

On the one hand, the elaborate steering of the antenna solves the contradiction between azimuth resolution and coverage extension. On the other hand, it results in the dependence of Doppler centroid on azimuth time. According to the acquisition geometry illustrated by Figure 1, the relation between instantaneous squint angle and azimuth time is given by

$$\theta_s = \theta_{s0} - vt\cos\theta_{s0}/\lambda R_{rot0} \tag{4}$$

The Doppler centroid of each point target is determined by the squint angle at beam center crossing time. Therefore, the variation rate of Doppler centroid with azimuth time can be written as follow

$$k_{rot} = \frac{df_d}{dt} = \frac{2v}{\lambda}\frac{d\sin\theta_s}{d}t = -\frac{2v^2\cos^2\theta_{s0}}{\lambda R_{rot0}} \tag{5}$$

This parameter is extremely important for squint sliding spotlight SAR, which represents the characteristic of the Doppler history. The Doppler history of several point targets with the same closest range is shown by Figure 2, and f_{d0} is the Doppler centroid of scene center, k_a is the Doppler rate of point target. It is clearly shown in Figure 2 that the total Doppler bandwidth is composed of two parts, B_{a0} and B_{a1}. B_{a0} is determined by the azimuth antenna width, i.e., the total Doppler bandwidth of strip-map mode, and B_{a1} represents the variation extension of Doppler centroid with azimuth time. It is shown that the shadow area in Figure 2, corresponding with the targets close to the edges of the illuminated zone, does not increase the total Doppler bandwidth. Consequently, the total Doppler bandwidth of point targets with the same closest range can be written as

$$B_a = B_{a0} + B_{a1} = 2v/D\cos\theta_{s0}|k_{rot}|T_I \tag{6}$$

where D represents the antenna length. For the sliding spotlight mode, B_{a1} is generally much more than B_{a0}.

Considering the dependence of Doppler centroid on slant range and the skew of two-dimensional spectrum arising from the squint

angle, the total Doppler bandwidth in two-dimensional frequency domain should be modified as

$$B_a = B_{a0} + B_{a1} + B_{a2} + B_{a3} \tag{7}$$

where B_{a2} denotes the variation extension of Doppler centroid with slant range, and B_{a3} denotes the skewed extension of Doppler spectrum. The analytic expression of B_{a2} is not available, and thus it should be estimated by numerical computation when the beam position of SAR system is designed. The B_{a3} can be approximated as

$$B_{a3} = 2vB_r \sin\theta_{s0}/c \tag{8}$$

where B_r is the bandwidth of transmitted chirp signal.

According with the Nyquist sampling theorem, the PRF must be more than the total Doppler bandwidth in order to avoid spectral folding. Unfortunately, high PRF means severe range ambiguity, huge data rate and constraint on imaging swath. Therefore, the PRF of sliding spotlight mode is typically kept the same as that adopted in strip-map mode, and azimuth spectral folding phenomenon is overcome utilizing the azimuth deramping pre-processing.

3. EXTENDED WDA

This section presents an extended WDA to focus highly squinted sliding spotlight SAR data. In extended WDA, the efficient azimuth deramping is adopted to eliminate the azimuth spectral folding, and the precise WDA is utilized to implement the residual and fine focusing. The process flow of extended WDA is shown in Figure 3, and the compensation terms will be derived in the following.

3.1. Azimuth Deramping Preprocessing

The azimuth deramping preprocessing is an azimuth-invariant filtering, which could overcome the azimuth spectral folding phenomenon and preserve the space-variant characteristics of the system transfer function. This filtering process is essentially a deramping based (SPECAN [1, 16], spectral analysis) processing, involving a chirp multiplication of the azimuth signal, a subsequent Fourier transform and residual phase cancellation. Moreover, its implementation in the discrete domain could be accelerated utilizing the FFT. The idea of azimuth deramping preprocessing in this paper is the same with that for broadside mode in [15]. However, the peculiarity of the squint mode should be particularly taken into account. The purpose of the multiplication of deramping phase is to minimize the total Doppler

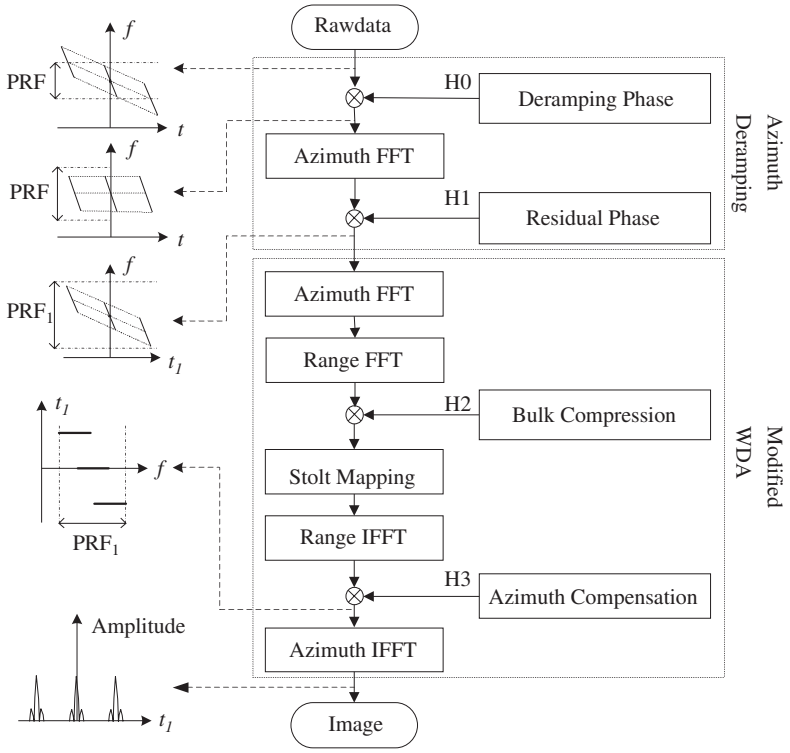

Figure 3. Process flow of extended WDA.

bandwidth. According to the analysis of the Doppler history in Section II, the deramping phase should be

$$H_0(t) = \exp\left\{-j\pi k_{rot} t^2\right\} \tag{9}$$

After the multiplication of the deramping phase, the total Doppler bandwidth becomes $(B_{a0} + B_{a2})$. Therefore, the system PRF should satisfy

$$\text{PRF} \geq B_{a0} + B_{a2} \tag{10}$$

This restrictive condition is differently with that in broadside mode given in [15], where PRF is only required to be more than B_{a0}.

Although the Fourier transform is adopted during the implementation of azimuth deramping, the signal after azimuth deramping still should be seen as time-domain signal. The PRF and the azimuth sampling interval should be updated as

$$\text{PRF}_1 = |k_{rot}| N_a / \text{PRF} \tag{11}$$

$$\Delta_{t1} = \text{PRF} / (|k_{rot}| N_a) \tag{12}$$

Thereby, the residual phase cancellation is implemented by

$$H_1(t_1) = \exp\left\{-j\pi k_{rot} t_1^2\right\} \tag{13}$$

While the azimuth deramping implements azimuth up-sampling, it preserves the Doppler history characteristic of point targets. If the new PRF is more than the total Doppler bandwidth, the azimuth spectral folding is overcome. According to formula (11), the system PRF and FFT length should satisfy

$$\mathrm{PRF} \leq N_a \left|k_{rot}\right| / B_a \tag{14}$$

where N_a is the azimuth FFT length. It is clearly that inequality (10) and (14) are opposite in the restriction on system PRF. when determining the system PRF, the inequality (10) should be satisfied firstly, and if the inequality (14) is not satisfied, the FFT length should be appropriately increased by limited zero padding. Consequently, the azimuth dimension extension of the focused image is determined by

$$T_{a1} = N_a/\mathrm{PRF}_1 = \mathrm{PRF}/|k_{rot}| \tag{15}$$

Evidently, T_{a1} is essentially independent of N_a, and only determined by PRF (k_{rot} is constant for a specific beam position). The required PRF in squint mode is higher than that in broadside mode, and the absolute value of k_{rot} in squint mode is smaller than that in broadside mode. And thus, the azimuth dimension extension of the focused image in squint mode is bigger than that in broadside mode, and generally, azimuth folding in focused image will not appear in squint mode.

3.2. Wavenumber Domain Algorithm

After the processing of azimuth deramping, the new PRF is higher than the total Doppler bandwidth. Therefore, the correlative imaging algorithm for highly squinted strip-map SAR can be extended to focus the highly squinted sliding spotlight SAR data. WDA is the most precise imaging algorithm compared with ECS, NCS, and NLCS. However, the conventional WDA is not suitable to process highly squinted SAR data because the Doppler parameters can't be updated along the range and the skew of 2-D spectrum after conventional Stolt mapping constrain the range dimension extension in focused image. So, we introduce the modified Stolt mapping in order to achieve the update of Doppler parameters along range and enlarge the range dimension extension in the focused image.

The phase for bulk compression is given by

$$\begin{aligned} H_2(f_\tau, f) \;=\; & \exp\left\{-j\pi f_\tau^2 / K_r\right\} \exp\left\{-j2\pi t_s f_\tau\right\} \\ & \exp\left\{\frac{4\pi r_c}{c}\sqrt{(f_0+f_\tau)^2 - (cf/2v)^2}\right\} \end{aligned} \tag{16}$$

where f_τ is the range frequency, $f_\tau \in [-B_r/2,\ B_r/2]$, f is the azimuth frequency, $f \in [f_{d0} - B_a/2,\ f_{d0} + B_a/2]$, t_s is the difference in time between the transmission of the pulse and the recording of the first sample of the associated echo. The second term in (16) can't be replaced with another formation, when the Stolt mapping is implemented by sinc interpolation. That's because that the sinc interpolation is based on the principle of low-pass filtering.

The conventional Stolt mapping [1] is

$$f_{\tau 0} = \sqrt{(f_0 + f_\tau)^2 - \left(\frac{cf}{2v}\right)^2} - f_0 \tag{17}$$

We apply the modified Stolt mapping, which can be written as

$$f_{\tau 1} = \sqrt{(f_0 + f_\tau)^2 - \left(\frac{cf}{2v}\right)^2} - \sqrt{f_0^2 - \left(\frac{cf}{2v}\right)^2} \tag{18}$$

Obviously, this modified Stolt mapping separates the residual azimuth compression from the conventional Stolt mapping. Consequently, the azimuth compression could be implemented in range-Doppler domain, and the Doppler parameters can be updated along range. Further investigation indicates that the variation extension of new range frequency based on the modified Stolt mapping is smaller than that based on conventional Stolt mapping. This result is more evident as the squint angle increase. Thus, the processing of highly squinted SAR data must adopt the modified Stolt mapping. The new range frequency should be defines as

$$f_{\tau 1} = \min(f_{\tau 1}) + n\Delta_{f_{\tau 1}} \quad n = 0, \ldots, N_r - 1 \tag{19}$$

$$\Delta_{f_{\tau 1}} = [\max(f_{\tau 1}) - \min(f_{\tau 1})]/N_r \tag{20}$$

where the length of range FFT is denoted as N_r, the sampling interval of range frequency is denoted as $\Delta_{f_{\tau 1}}$. Thus, the system sampling frequency is updated as

$$F_{s1} = N_r \Delta_{f_{\tau 1}} \tag{21}$$

Then, the range dimension extension in focused image can be expressed as

$$T_{r1} = N_r F_{s1} = 1/\Delta_{f_{\tau 1}} \tag{22}$$

After the modified Stolt mapping and range IFFT, we get the signal in range-Doppler domain, and the azimuth compensation can

be achieved by the following phase

$$H_3(\tau_1, f) = \exp\left\{\frac{4\pi(r-r_c)}{c}\sqrt{(f_0+f_\tau)^2-\left(\frac{cf}{2v}\right)^2}\right\} \exp\left\{j\left(\frac{2\pi r_c \tan\theta_{s0}}{c}+\frac{2\pi f_{d0}}{k_{rot}}\right)f\right\}\exp\left\{-\pi\frac{f^2}{k_{rot}}\right\} \quad (23)$$

The first term in (23) is for residual azimuth compression, the second term is applied to correct the azimuth geometry aberration, and the third term cancel the residual phase arising from the azimuth deramping preprocessing. It is deserved to note that the range sampling interval should be computed according to (21) and the Doppler parameters should be updated along with the freshly-defined range gate.

After azimuth IFFT, the SAR image is obtained, and the point target is located in $((r-r_c), vt_n)$.

Table 1. Simulation parameters.

Parameter	Value
Carrier wavelength	0.03 m
Platform velocity	200 m/s
Platform height	10000 m
Look angle	50°
Squint angle at center time	50°
Pulse bandwidth	300 MHz
Pulse repetition frequency	500 Hz
Antenna length	2 m
Mode factor	0.5

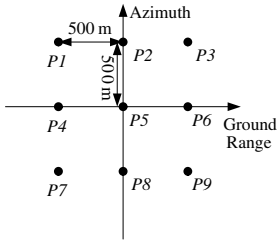

Figure 4. Simulation Scene.

Figure 5. SAR image of point targets.

4. SIMULATION EXPERIMENTS

To demonstrate the validities of the proposed algorithm, the highly squinted sliding spotlight SAR raw data of nine point targets were simulated. The specific simulation parameters are shown in Table 1. The simulation scene is illustrated by Figure 4. The corresponding SAR image of the point targets is shown in Figure 5. Figure 6 gives the interpolated contour plots of the focused targets. And the quality of imaging of these point targets using extended WDA is shown in Table 2. The contour plots and quality analysis results indicate that the focusing performance of extended WDA is satisfactory.

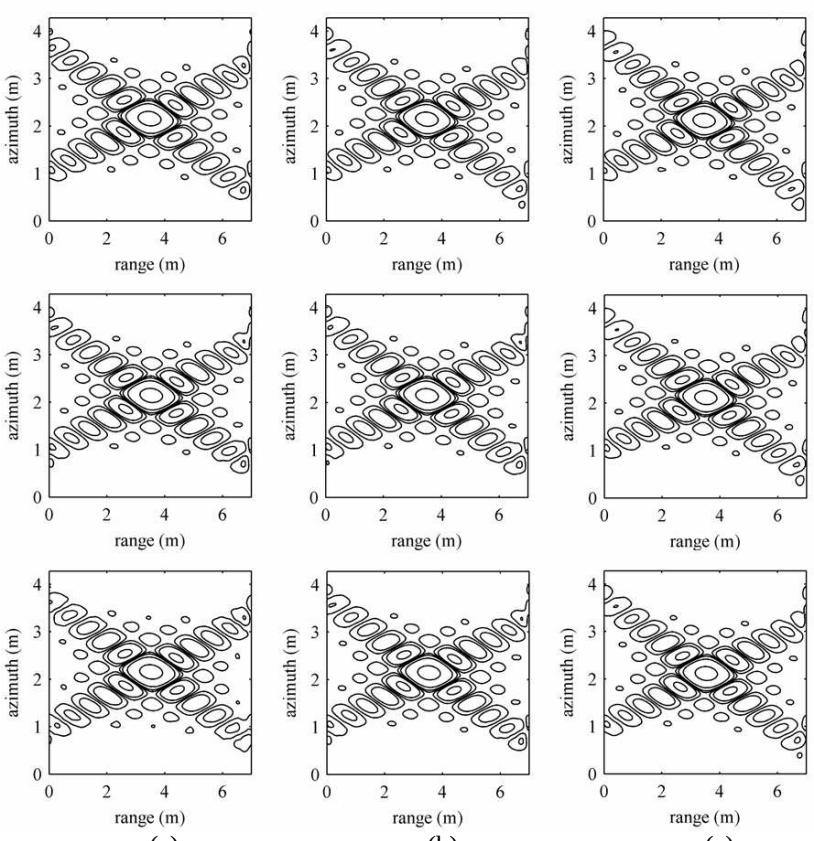

Figure 6. Contour plots showing the processing results of nine point targets located at (a) near, (b) mid-, and (c) far range. Contour lines at -3, -15, -25, and -35 dB.

Table 2. Imaging qualities analysis of point targets.

target	range		azimuth	
	PSLR/dB	ISLR/dB	PSLR/dB	ISLR/dB
$P1$	−13.27	−10.58	−13.29	−10.60
$P2$	−13.27	−10.61	−13.28	−10.54
$P3$	−13.29	−10.66	−13.25	−10.52
$P4$	−13.28	−10.56	−13.35	−10.74
$P5$	−13.28	−10.58	−13.27	−10.52
$P6$	−13.27	−10.61	−13.26	−10.52
$P7$	−13.23	−10.54	−13.29	−10.62
$P8$	−13.28	−10.58	−13.27	−10.55
$P9$	−13.27	−10.59	−13.27	−10.52

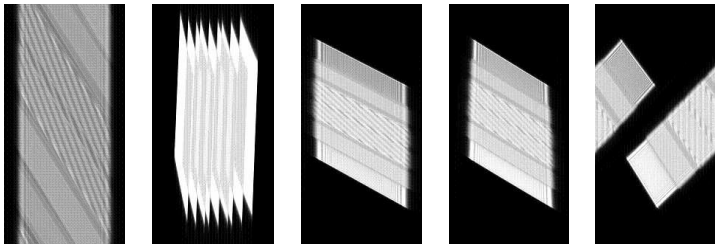

Figure 7. Processing results of extended WDA. (a) 2D spectrum of raw echo data. (b) Signal in two dimension time after azimuth deramping. (c) 2D spectrum after azimuth deramping. (d) 2D spectrum after modified Stolt mapping. (e) 2D spectrum of focused image using the extended WDA.

In order to demonstrate the effectiveness of the principle of choosing PRF, we presents the proper intermediate processing results of extended WDA, which is shown in Figure 7. When the PRF is chosen as 400 Hz, the wrap around appears in azimuth time domain, shown in Figure 8(a). Consequently, the 2D spectrum after azimuth deramping, shown in Figure 8(b), contains smearing, although the new azimuth frequency is higher than the total Doppler bandwidth. Figure 7(c) and Figure 7(d) demonstrate that the modified Stolt mapping hardly alter the profile of the 2D spectrum. However, the 2D spectrum after conventional Stolt mapping, illustrated by Figure 9, indicates that the conventional Stolt mapping induces the severe skew of 2D spectrum.

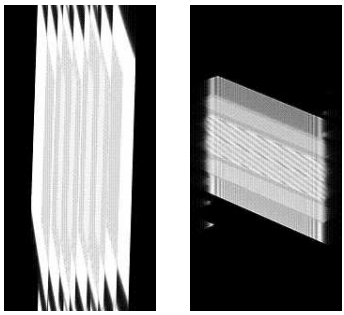

(a) (b)

Figure 8. Results after azimuth deramping with unsuitable PRF.

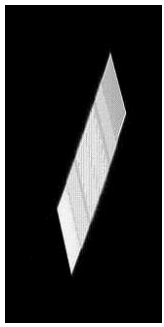

Figure 9. 2D spectrum after conventional Stolt mapping.

5. CONCLUSIONS

This paper presents an extended WDA for highly squinted sliding spotlight SAR data processing. The approach of azimuth deramping is applied to overcome the azimuth folding phenomenon. According to the analysis of the Doppler history and the method of azimuth deramping, the chirp rate for azimuth deramping should be identical with the rate of Doppler centroid varying; the PRF should be higher than the sum of the instantaneous Doppler bandwidth and the variation extension of Doppler centroid with slant range; the updated PRF should be higher than the total Doppler bandwidth. Through azimuth deramping, the azimuth extension of focused image is in proportion to PRF and in inverse proportion to the chirp rate for azimuth deramping. Precise de-coupling of highly squinted sliding spotlight SAR data is achieved by modified WDA, in which modified Stolt mapping is applied to enlarge the range extension of focused image and update the Doppler parameters along range. Improved time-shift term in match filtering is necessary for the perfect implementation of Stolt mapping using sinc interpolation. Accurate azimuth compensation term confirm the correctness of azimuth position of targets in focused image.

Future work includes the system design, real-time processing [22], motion compensation [1], and the approach of beamforming [23] for decreasing the variation of Doppler centroid with range. It is worthy to note that multi-channel technique [24] is an excellent solution to decrease the system required PRF at the cost of system increasing complexity.

ACKNOWLEDGMENT

The authors would like to thank the anonymous reviewers for their valuable comments and useful suggestions. This work was supported in part by the Chinese National Natural Science Foundation under contract No. 60901055, and the Aeronautical Science Foundation under contract No. 20090151001.

REFERENCES

1. Cumming, I. G. and F. H. Wong, *Digital Processing of Synthetic Aperture Radar Data: Algorithms and Implementation*, Artech House, Norwood, MA, 2005.
2. Chan, Y. K. and V. C. Koo, "An introduction to Synthetic Aperture Radar (SAR)," *Progress In Electromagnetics Research B*, Vol. 2, 27–60, 2008.
3. Mao, X., D. Y. Zhu, and Z. D. Zhu, "Signatures of moving target in polar format spotlight SAR image," *Progress In Electromagnetics Research*, Vol. 92, 47–64, 2009.
4. Zhao, Y. W., M. Zhang, and H. Chen, "An efficient ocean SAR raw signal simulation by employing fast Fourier transform," *Journal of Electromagnetic Waves and Applications*, Vol. 24, No. 16, 2273–2284, 2010.
5. Park, J.-I. and K.-T. Kim, "A comparative study on isar imaging algorithms for radar target identification," *Progress In Electromagnetics Research*, Vol. 108, 155–175, 2010.
6. Belcher, D. P. and C. J. Baker, "High resolution processing of hybrid strip-map/spotlight mode SAR," *IEE Proc. — Radar, Sonar Navig.*, Vol. 143, No. 6, 366–374, 1996.
7. Jin, M. and C. Wu, "A SAR correlation algorithm which accommodates large range migration," *IEEE Trans. Geosci. Remote Sens.*, Vol. 22, No. 6, 592–597, 1984.
8. Raney, R. K., H. Runge, R. Bamler, I. G. Cumming, and F. H. Wong, "Precision SAR processing using chirp scaling," *IEEE Trans. Geosci. Remote Sens.*, Vol. 32, No. 4, 786–799, 1994.
9. Cafforio, C., C. Prati, and F. Rocca, "SAR data focusing using seismic migration techniques," *IEEE Trans. Aerosp. Electron. Syst.*, Vol. 27, No. 2, 194–207, 1991.
10. Lanari, R., "A new method for the compensation of the SAR range cell migration based on the chirp-z transform," *IEEE Trans. Geosci. Remote Sens.* Vol. 33, No. 5, 1296–1299, 1995.
11. Sun, J., S. Mao, G. Wang, and W. Hong, "Polar format algorithm

for spotlight bistatic SAR with arbitrary geometry configuration," *Progress In Electromagnetics Research*, Vol. 103, 323–338, 2010.

12. Mittermayer, J., R. Lord, and E. Borner, "Sliding spotlight SAR processing for TerraSAR-X using a new formulation of the extended chirp scaling algorithm," *Proc. of IGARSS*, 1462–1464, 2003.
13. Prats, P., R. Scheiber, J. Mittermayer, A. Meta, and A. Moreira, "Processing of sliding spotlight and TOPS SAR data using baseband azimuth scaling," *IEEE Trans. Geosci. Remote Sens.*, Vol. 48, No. 2, 770–780, 2010.
14. Jia, X., Y. Deng, W. Xu, and L. Feng, "Processing of sliding spotlight SAR data using the azimuth frequency deramping," *Proc. of EUSAR*, 627–630, 2010.
15. Lanari, R., S. Zoffoli, E. Sansosti, G. Fornaro, and F. Serafino, "New approach for hybrid strip-map/spotlight SAR data focusing," *IEE Proc. — Radar, Sonar Navig.*, Vol. 148, No. 6, 363–372, 2001.
16. Nie, X., D. Y. Zhu, and Z. D. Zhu, "Application of synthetic bandwidth approach in SAR polar format algorithm using the deramp technique," *Progress In Electromagnetics Research*, Vol. 80, 447–460, 2008.
17. Moreira, A. and Y. Huang, "Airborne SAR processing of highly squinted data using a chirp scaling approach with integrated motion compensation," *IEEE Trans. Geosci. Remote Sens.*, Vol. 32, No. 5, 1029–1040, 1994.
18. Davidson, G. W., I. G. Cumming, and M. R. Ito, "A chirp scaling approach for processing squint mode SAR data," *IEEE Trans. Aerosp. Electron. Syst.*, Vol. 32, No. 1, 121–133, 1996.
19. Wong, F. H. and T. S. Yeo, "New applications of the nonlinear chirp scaling in SAR data processing," *IEEE Trans. Geosci. Remote Sens.*, Vol. 39, No. 5, 946–953, 2001.
20. Yeo, T. S., N. L. Tan, C. Zhang, and Y. Lu, "A new subaperture approach to high squint SAR processing," *IEEE Trans. Geosci. Remote Sens.*, Vol. 39, No. 5, 954–968, 2001.
21. Reigber, A., E. Alivizatos, A. Potsis, and A. Moreira, "Extended wavenumber domain synthetic aperture radar focusing with integrated motion compensation," *IEE Proc. — Radar Sonar Navig.*, Vol. 153, No. 3, 301–310, 2006.
22. Chan, Y. K., V. C. Koo, B.-K. Chung, and H.-T. Chuah, "Modified algorithm for real time SAR signal processing," *Progress In Electromagnetics Research C*, Vol. 1, 159–168, 2008.

23. Lim, S.-H., J.-H. Han, S.-Y. Kim, and N.-H. Myung, "Azimuth beam pattern synthesis for airborne SAR system optimization," *Progress In Electromagnetics Research*, Vol. 106, 295–309, 2010.
24. Ma, L., Z.-F. Li, and G. S. Liao, "System error analysis and calibration methods for multi-channel SAR," *Progress In Electromagnetics Research*, Vol. 112, 309–327, 2011.